

Supporting Information

Electroreduction of Co^{II} Coordination Complex Producing Metal-Organic Film with High Performance Toward Electrocatalytic Hydrogen Evolution

Leticia S. Bezerra^a, Persiely P. Rosa^b, Guilherme V. Fortunato^a, Lucas Pizzuti^b, Gleison A. Casagrande^{b}, Gilberto Maia^{a*}*

- a) Instituto de Química, Universidade Federal de Mato Grosso do Sul; Av. Senador Filinto Muller, 1555; Campo Grande, MS 79074-460, Brazil.
- b) Grupo de Pesquisa em Síntese e Caracterização Molecular do Mato Grosso do Sul, Instituto de Química, Universidade Federal de Mato Grosso de Mato Grosso do Sul (laboratório 2), Av. Senador Filinto Muller 1555, Campo Grande, MS 79074-460, Brazil.

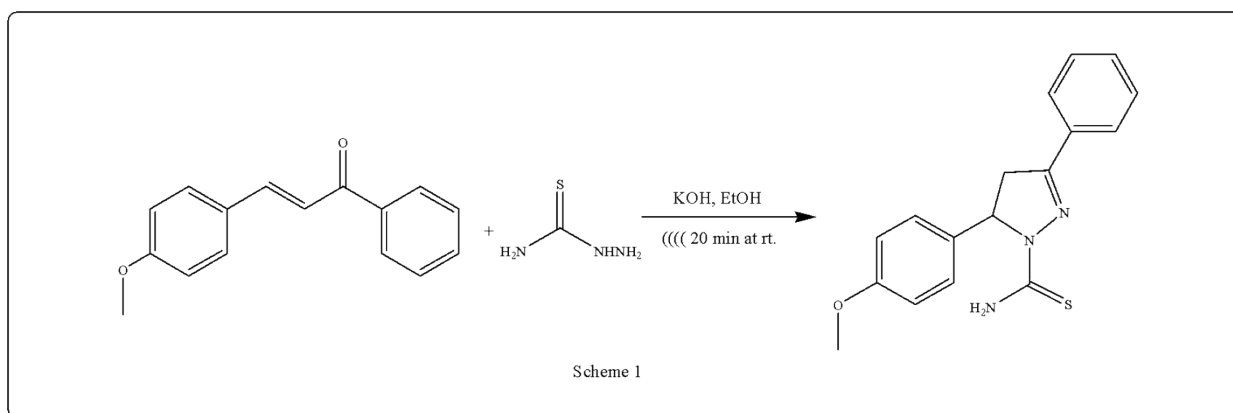
* Corresponding authors: gleison.casagrande@ufms.br and gilberto.maia@ufms.br

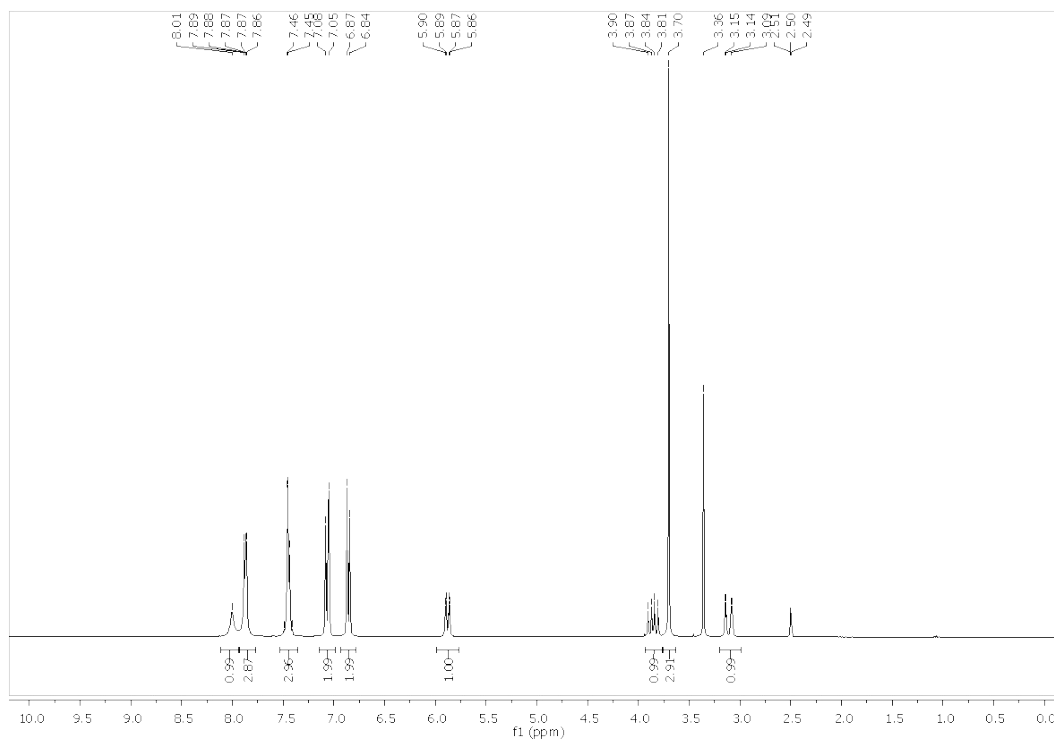
Synthesis of the Co^{II} complex and Ligand.

Ligand (L) synthesis.

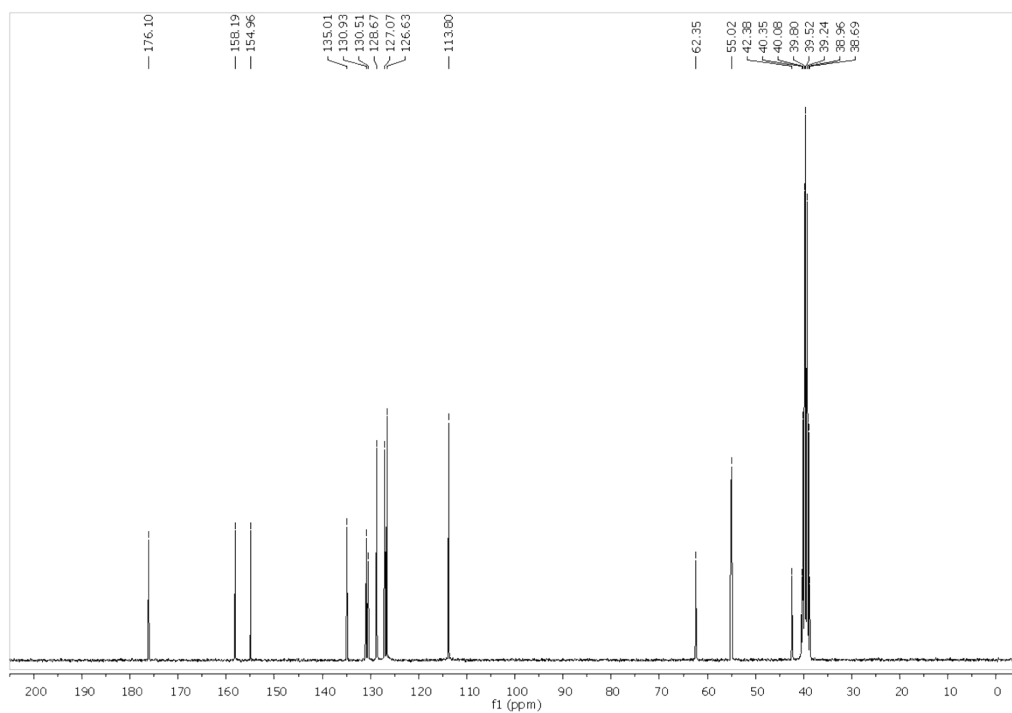
The ligand (L = 1-thiocarbamoyl-5-(4-methoxyphenyl)-3-phenyl-4,5-dihydro-1*H*-pyrazole) was synthesized *via* cyclocondensation reaction of chalcone with thiosemicarbazide in the presence of potassium hydroxide under ultrasonic conditions as described in the literature [1] (Scheme S1). In a 25 mL beaker, the 3-(4-methoxyphenyl)-1-phenylprop-2-en-1-one (chalcone) (2.0 mmol, 0.48 g) and thiosemicarbazide (4.0 mmol, 0.36 g) were mixed in EtOH (10 mL) and KOH (4.0 mmol, 0.22 g) was added. The reaction mixture was then sonicated by an ultrasonic probe with a frequency of 20 KHz at room temperature (25 °C). The complete consumption of chalcone occurred after 20 min, as monitored through the GC. The crude product was allowed to cool in a refrigerator. The precipitate obtained was filtered through a Buchner funnel under vacuum, washed with cold water and dried under high-vacuum. Afterwards, the ligand was obtained as a pure crystalline compound by recrystallization in hot ethanol. Ligand data: Yield 0.45 g (73%); Melting Point 172 °C; C₁₇H₁₇N₃OS, MW 311.40 g mol⁻¹. IR (KBr): ν (cm⁻¹) 3376–3366 (N–H), 1600–1444 (C=N + (C=C), 1378 (C=S), 1243 (C–O), 1169 (C–C), 1031 (C–H), 699 and 575 (C–H and C–C)_{bending}; ¹H NMR (300 MHz, DMSO-*d*₆): δ 8.01 (bs, 1H, NH), 7.93–7.77 (m, 3H, Ar and NH), 7.53–7.36 (m, 3H, Ar), 7.07 (m, 2H, Ar), 6.86 (m, 2H, Ar), 5.88 (dd, *J* = 11.2, 3.1 Hz, 1H), 3.86 (dd, *J* = 18.0, 11.3 Hz, 1H), 3.70 (s, 3H, OMe), 3.11 (dd, *J* = 18.0, 3.3 Hz, 1H); ¹³C NMR (75 MHz, DMSO-*d*₆): δ 176.1, 158.2, 155.0, 135.0, 130.9, 130.5, 128.7, 127.1, 126.6, 113.8, 62.3, 55.0, 42.4 (Figure S1).

Scheme S1. Synthesis of the ligand (1-thiocarbamoyl-5-(4-methoxyphenyl)-3-phenyl-4,5-dihydro-1*H*-pyrazole).





^1H NMR (300 MHz, DMSO-d_6) for the Ligand



^{13}C NMR (75 MHz, DMSO-d_6) for the Ligand

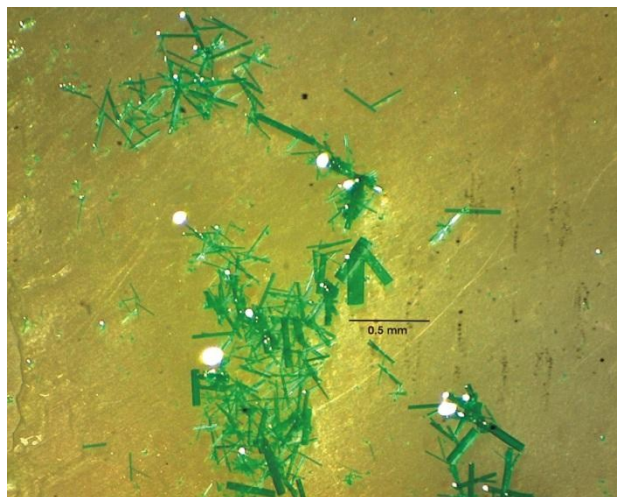
Figure S1. ^1H NMR and ^{13}C NMR spectra for the Ligand.

Co^{II}(L)₂Cl₂ synthesis

The cobalt complex (Co^{II}(L)₂Cl₂) was prepared by reacting the CoCl₂·6H₂O and the ligand (L) according to the methods reported in the literature [2,3]. 0.4 mmol (0.1245 g) of the ligand was added to a pink solution containing 0.2 mmol (0.0475 g) of Cobalt(II) chloride hexahydrate in a mixture of solvent (10 mL acetone/ 4 mL acetonitrile). This solution was maintained under magnetic stirring at room temperature for 3 h. Subsequently, a green solid was obtained and the solution was filtered off. Suitable crystals for X-Ray analysis were obtained by recrystallization of this green solid in a mixture (1:1;V/V) of dichlorometane/acetone through slow solvent evaporation (Figure S2). Yield: 78% (0.1341 g) of crystals based on the Co^{II} salt used; Melting Point: 203-204 °C; FW = 752.62 (C₃₄H₃₄Cl₂CoN₆O₂S₂): Calc. (%) C 54.26; H 4.55, N 11.17; Found (%) C 54,13; H 4,45; N 11,07. IR (KBr, v/cm⁻¹): 3401-3269 [ν(N-H)], 3120 [ν(C-H_{ar.})], 2944 [ν(CH₂)], 1600 [ν(C=N_{ring})], 1526-1446 [ν(C=C)], 1351 [ν(C=S)], 1245 [ν(H₃C-O)], 1028 [δ(C-H)], 770-580 [δ(C=C + C-H)]_{bending}.



Green solid obtained from the synthesis



Single crystals obtained after recrystallization

Figure S2. Photos for green solid obtained from the synthesis and after recrystallization. Authors' photographs.

Table S1. Crystal data and structure refinement for the complex.

Empirical formula	C ₃₄ H ₃₄ Cl ₂ CoN ₆ O ₂ S ₂	
Formula weight	752.62	
Temperature	296(2) K	
Wavelength	0.71073 Å	
Crystal system	Trigonal	
Space group	R3c	
Unit cell dimensions	a = 30.9254(9) Å	α = 90°.
	b = 30.9254(9) Å	β = 90°.
	c = 19.3130(14) Å	γ = 120°.
Volume	15996.0(15) Å ³	
Z	18	
Density (calculated)	1.406 Mg/m ³	
Absorption coefficient	0.790 mm ⁻¹	
F(000)	7002	
Crystal size	0.270 x 0.030 x 0.010 mm	
Theta range for data collection	1.317 to 26.405°.	
Index ranges	-35 ≤ h ≤ 38, -38 ≤ k ≤ 34, -14 ≤ l ≤ 24	
Reflections collected	38635	
Independent reflections	6059 [R(int) = 0.0913]	
Completeness to theta = 25.242°	99.9 %	
Data / restraints / parameters	6059 / 1 / 426	
Goodness-of-fit on F ²	1.010	
Final R indices [I > 2σ(I)]	R1 = 0.0457, wR2 = 0.0845	
R indices (all data)	R1 = 0.1178, wR2 = 0.1061	
Largest diff. peak and hole	0.250 and -0.221 e.Å ⁻³	
R1 = Σ Fo - Fc / Σ Fo ; wR2 = Σ[w(Fo ² - Fc ²) ² / Σ(wFo ²)] ^{-1/2}		

Table S2. Selected bond lengths [\AA] and angles [$^\circ$] for the Co^{II} complex.

Co-Cl(1)	2.242(2)
Co-Cl(2)	2.251(3)
Co-S(2)	2.327(2)
Co-S(1)	2.333(2)
Co \cdots N(4)	3.464(6)
Co \cdots N(3)	3.441(7)
Cl(1)-Co-Cl(2)	109.27(11)
Cl(1)-Co-S(2)	111.68(11)
Cl(2)-Co-S(2)	114.44(11)
Cl(1)-Co-S(1)	115.94(10)
Cl(2)-Co-S(1)	109.13(10)
S(2)-Co-S(1)	96.01(7)
N(3) \cdots Co \cdots N(4)	172.06(10)

Table S3. Intramolecular hydrogen bonds for the Co^{II} complex [\AA and $^\circ$].

D-H \cdots A	d(D-H)	d(H \cdots A)	d(D \cdots A)	$\angle(\text{DHA})$
N(4)-H(4b) \cdots Cl(2)	0.86	2.48	3.305(7)	158.8
N(3)-H(3b) \cdots Cl(1)	0.86	2.44	3.255(8)	158.3

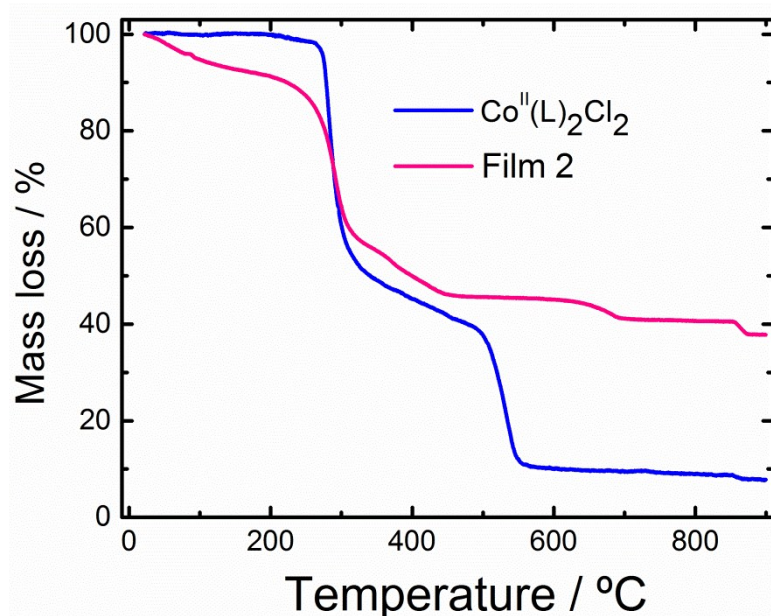


Figure S3. TG responses for the burning of $\text{Co}^{\text{II}}(\text{L})_2\text{Cl}_2$ and Film 2.

Complementary information on ICP OES determination of Co and S

Table S4 shows the detection limits (DLs) calculated according to the IUPAC recommendations as 3 times the standard deviation of the blank signal (BS) divided by the slope of the calibration curve (m): $DL = 3 \times BS / m$. The quantification limits (QL) were calculated in the same way, with $n = 15$, $QL = 10 \times BS / m$. The linear range of the calibration curve was 0.00 - 5.00 mg L⁻¹. Addition and recovery tests to verify the accuracy of the proposed method as % RSD (relative standard deviation) were performed for solutions containing 0.05 and 0.50 mg L⁻¹ according to table S5.

Table S4 - Figures of merits for each analyte obtained by ICP OES

Element	Linear equation	R ²	DL (mg/L)	QL (mg/L)
Co	$I = 3366C + 113.89$	0.9998	0.0006	0.002
S	$I = 209.884C + 15.05$	0.9997	0.002	0.007

Table S5 - Addition and recovery tests to verify the accuracy of the method used for all analytes obtained by ICP OES (All concentrations are in mg L⁻¹ and $n = 3$).

Element	Added (mg L ⁻¹)	Determination (mg L ⁻¹)	Recovery %	%RSD
Co	0.050	0.050	100.00	0.89
	0.500	0.499	99.80	0.18
S	0.050	0.049	98.90	0.95
	0.500	0.507	101.40	0.42

After certification of the quantification method used, the quantification of the cobalt and sulfur present in the Film 2 according to table S6 was performed.

Table S6 - Results of the analytes present in the Film 2, obtained by ICP OES. (All concentrations are in % m.m⁻¹ and $n = 3$).

Analyte	Amount in the Film 2
Co	38.54 ±0.43
S	3.38 ±0.03

Table S7. EDX results based on HAADF-STEM mapping image for the Film 2 in Figure 4D.

Element	Peak Area	Area Sigma	k factor	Abs Corr.	Weight %	Weight % Sigma	Atomic %
S K	1452	98	0.959	1.000	6.35	0.41	11.02
Cl K	190	63	0.983	1.000	0.85	0.28	1.33
Co K	16149	227	1.261	1.000	92.80	0.48	87.65
Totals					100.00		

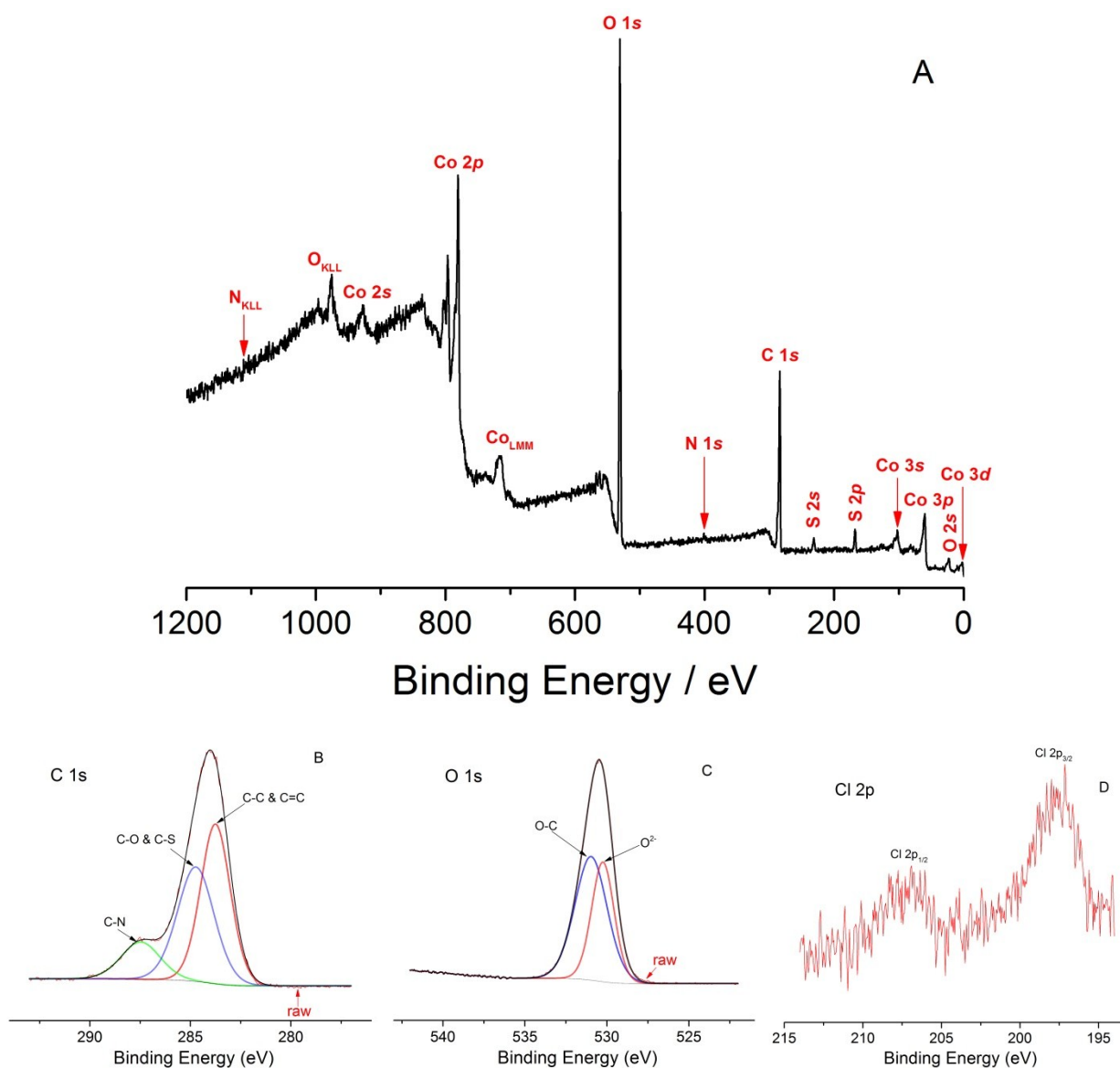


Figure S4. XPS spectrum of Film 2 (A). High-resolution C 1s (B), O 1s (C), and Cl 2p (D) XPS spectra of Film 2.

Table S8. Positions, relative sensitive factors (R.S.F.), atomic and mass percentages obtained from the XPS spectrum shown in Figure S4.

Name	Position (eV)	R.S.F.	Content (at. %)	St. Dev.	Content (mass %)
Co 2p	780.0	12.62	10.33	0.30	31.99
C 1s	284.0	1	48.67	0.563	30.70
O 1s	530.5	2.93	37.20	0.44	31.26
S 2p	168.0	1.68	3.44	0.32	5.80
N 1s	401.0	1.8	0.36	0.16	0.26
Cl 2p	-	-	-	-	-

Table S9. Positions and percentages of content of functional groups presents on Film 2 obtained from high-resolution XPS spectra shown in Figures S4 and 6.

Name	Group	Position (eV)	% content
C 1s	C-C; C=C	283.8	45.63
	C-O; C-S	284.7	40.45
	C-N	287.5	13.92
O 1s	O ²⁻	530.2	40.33
	O-C	531.0	59.67
S 2s	S-Co	162.0	8.96
	S=C	166.9	19.72
	S Oxidized	168.0	71.32
N 1s	N-C	398.5	31.72
	N-H	401.2	42.23
	N-N	402.6	5.54
	Nox	406.1	20.51

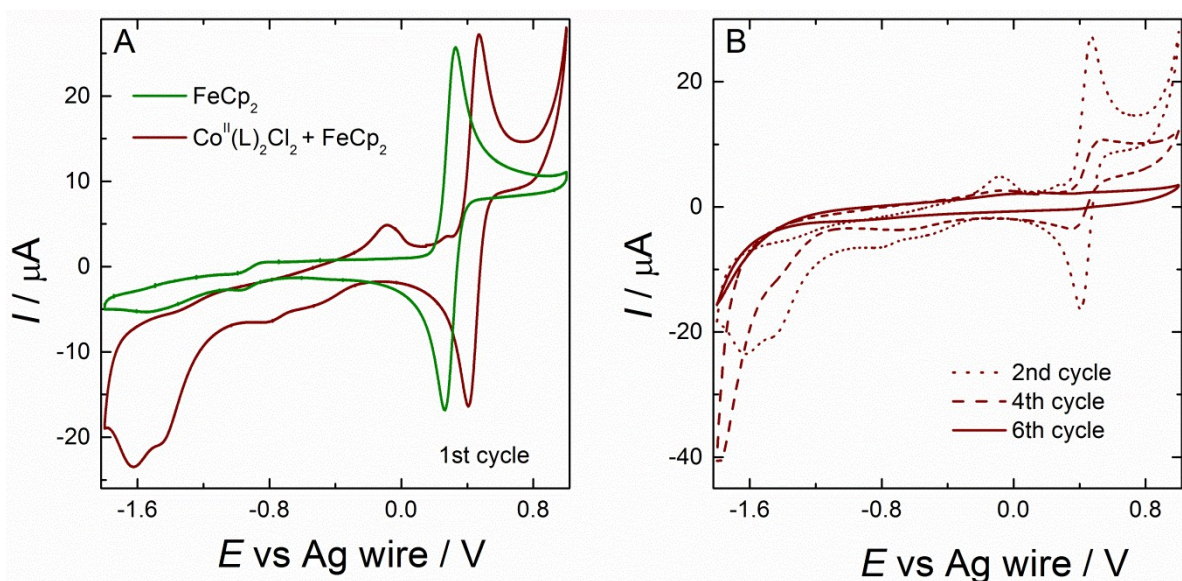


Figure S5. Cyclic voltammograms for bare GC in the presence of 0.5 mM FeCp₂ or 0.5 M Co^{II}(L)₂Cl₂ + 0.5 mM FeCp₂ in N₂-saturated 0.1 M TBAClO₄/ACN (1st cycle (A)) and 2nd to 6th cycles (B) to 0.5 M Co^{II}(L)₂Cl₂ + 0.5 mM FeCp₂ in N₂-saturated 0.1 M TBAClO₄/ACN. Potential scan rate: 20 mV s⁻¹. Potential scans begin at 0.15 V (positive direction).

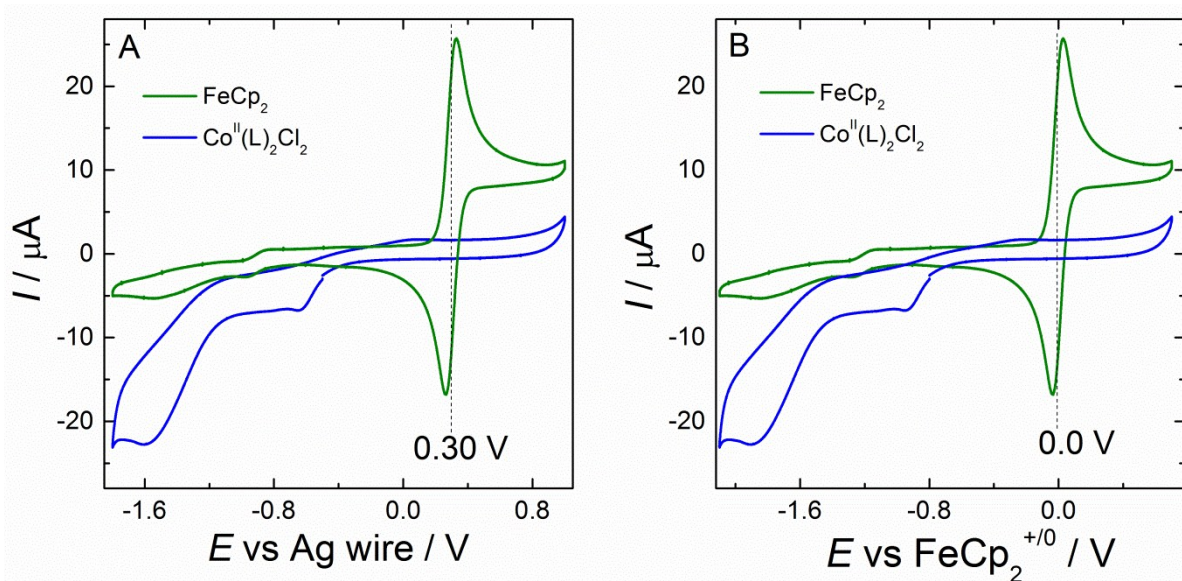


Figure S6. Cyclic voltammograms for bare GC in the presence of 0.5 mM FeCp₂ or 0.5 M Co^{II}(L)₂Cl₂ in N₂-saturated 0.1 M TBAClO₄/ACN. Potential scan rate: 20 mV s⁻¹. Potential scans begin at 0.15 V (positive direction) for FeCp₂ and -0.50 V (negative direction) for Co^{II}(L)₂Cl₂ at (A); potential scans begin at -0.15 V (positive direction) for FeCp₂ and -0.80 V (negative direction) for Co^{II}(L)₂Cl₂ at (B).

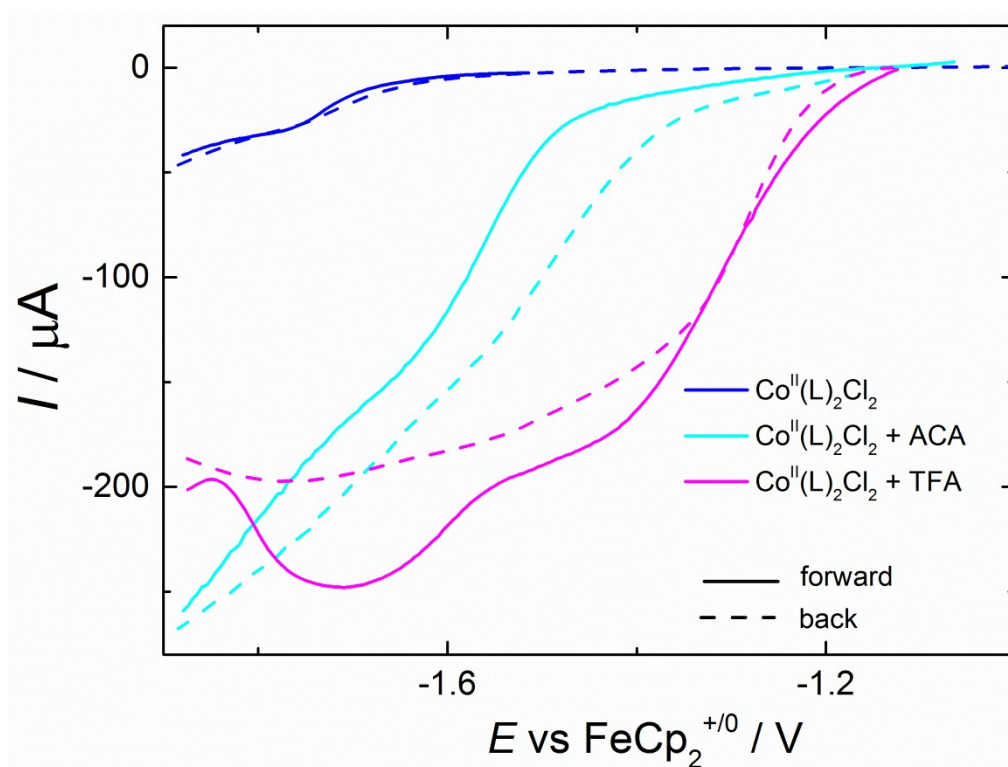


Figure S7. Hydrodynamic cyclic voltammograms for 0.5 mM $\text{Co}^{\text{II}}(\text{L})_2\text{Cl}_2$, 0.5 mM $\text{Co}^{\text{II}}(\text{L})_2\text{Cl}_2 + 0.5$ mM ACA, and 0.5 mM $\text{Co}^{\text{II}}(\text{L})_2\text{Cl}_2 + 0.5$ mM TFA in N_2 -saturated 0.1 M $\text{TBAClO}_4/\text{ACN}$ at $v = 10 \text{ mV s}^{-1}$ and 600 rpm. Potential scans begin at -1.00 V (negative direction).

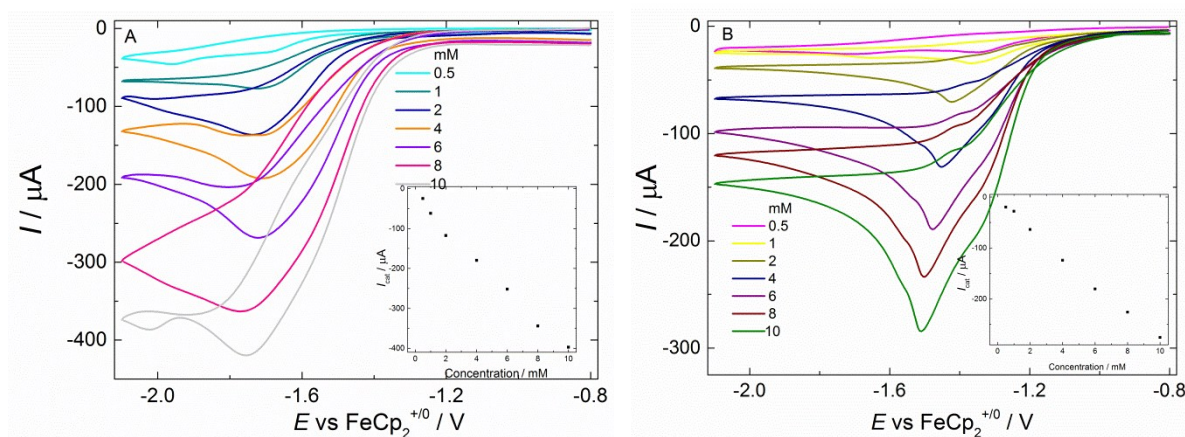


Figure S8. A) Cyclic voltammograms for bare GC in the presence of 0.5 mM $\text{Co}^{\text{II}}(\text{L})_2\text{Cl}_2 +$ different concentrations of ACA. Inset: Cathodic catalytic peak currents as a function of ACA concentration. B) Cyclic voltammograms for bare GC in the presence of 0.5 mM $\text{Co}^{\text{II}}(\text{L})_2\text{Cl}_2 +$ different concentrations of TFA. Inset: Cathodic catalytic peak currents vs. TFA concentration. All experiments were conducted in N_2 -saturated 0.1 M $\text{TBAClO}_4/\text{ACN}$, with a polished surface for bare GC prior to the beginning of each CV. Potential scan rate: 20 mV s^{-1} . Potential scans begin at -0.80 V (negative direction).

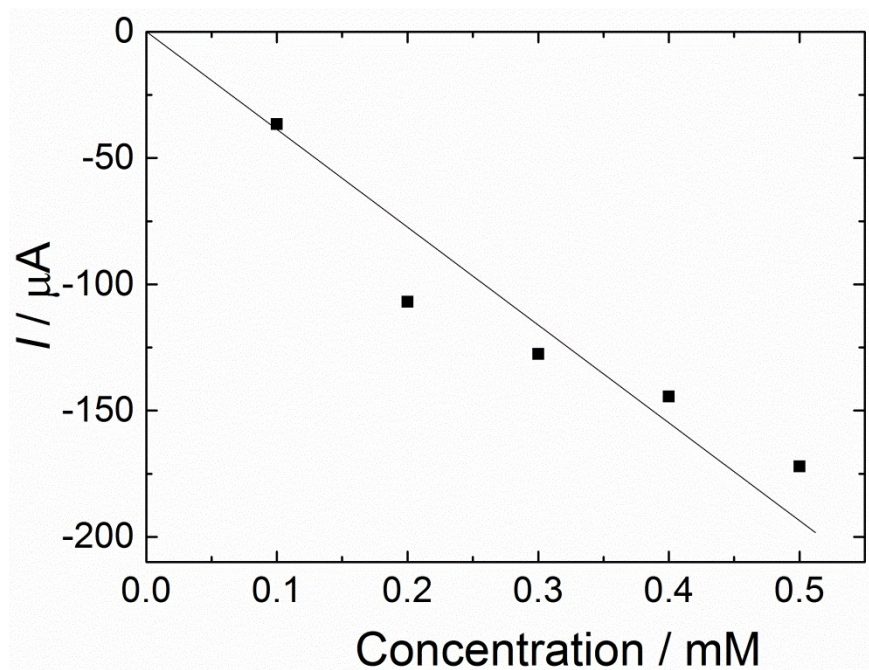


Figure S9. Cathodic catalytic peak currents as a function of $\text{Co}^{\text{II}}(\text{L})_2\text{Cl}_2$ concentration obtained from CV curves in N_2 -saturated 0.1 M $\text{TBAClO}_4/\text{ACN}$ containing 10 mM TFA, with a polished surface for bare GC prior to the beginning of each CV. Potential scan rate: 20 mV s^{-1} . Potential scans begin at -0.80 V (negative direction).

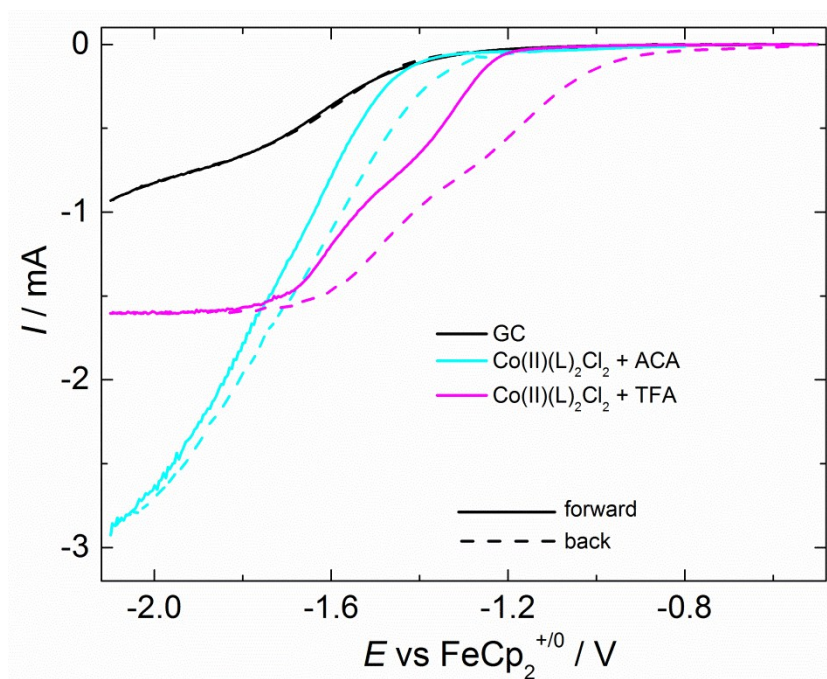


Figure S10. Hydrodynamic cyclic voltammograms for bare GC in the presence of 10 mM TFA, 0.5 mM $\text{Co}^{\text{II}}(\text{L})_2\text{Cl}_2 + 10 \text{ mM ACA}$, and 0.5 mM $\text{Co}^{\text{II}}(\text{L})_2\text{Cl}_2 + 10 \text{ mM TFA}$ in N_2 -saturated 0.1 M $\text{TBAClO}_4/\text{ACN}$ at $\nu = 10 \text{ mV s}^{-1}$ and 600 rpm. Potential scans begin at -0.50 V (negative direction).

Comments about usefulness of eq. 5 as well as the determination of overpotential (eq. 6)

As pointed out by McCarthy *et al.* [4], the usefulness of eq. 5 has been questioned [5] as a result of its dependence on multiple phenomena, including homoconjugation, which can affect several acids in ACN at the normally applied concentrations, and the thermodynamics of acid reduction to H₂. [5-7] Admittedly though, equation 5 is deemed suitable for our purposes.

As stated by Appel and Helm, [7] the most suitable potential for the determination of overpotential (eq. 6)— defined as the difference between equilibrium potential (thermodynamic potential), in the presence of the reaction H⁺/H₂, and the potential to which the catalyst works in a specific condition, resulting in a specific current [7] — is at $I_{cat/2}$, which is referred to as $E_{cat/2}$ (potential coupled with the specific catalytic rate). The reason being that the use of $E_{cat/2}$ results in lower potential variations given the variation in I_{cat} , a fact regarded essentially important for less-ideally behaved systems, [7] like that shown in Figure S12.

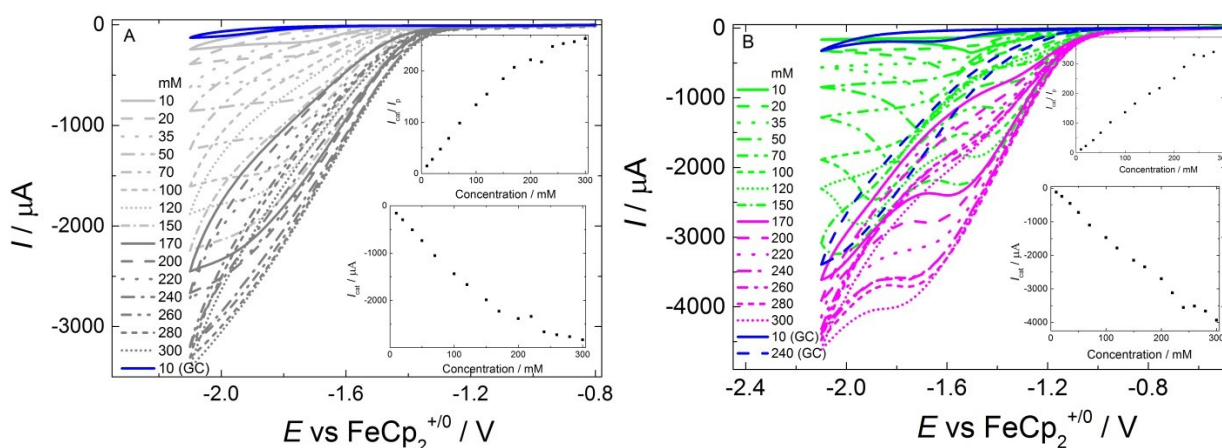


Figure S11. A) Cyclic voltammograms for bare GC in the presence of 0.5 mM Co^{II}(L)₂Cl₂ + different concentrations of ACA and bare GC in the presence of 10 mM ACA. Insets: Cathodic catalytic peak currents and normalized cathodic catalytic peak currents per cathodic peak current for 0.5 mM Co^{II}(L)₂Cl₂ in relation to ACA concentration. B) Cyclic voltammograms for bare GC in the presence of 0.5 mM Co^{II}(L)₂Cl₂ + different concentrations of TFA and bare GC in the presence of 10 and 240 mM TFA. Inset: Cathodic catalytic peak currents and normalized cathodic catalytic peak currents per cathodic peak current for 0.5 mM Co^{II}(L)₂Cl₂ in relation to TFA concentration. All experiments were performed in N₂-saturated 0.1 M TBAClO₄/ACN, with a polished surface for bare GC prior to the beginning of each CV. Potential scan rate: 20 mV s⁻¹. Potential scans begin at -0.80 in (A) and -0.50 in (B) (negative direction).

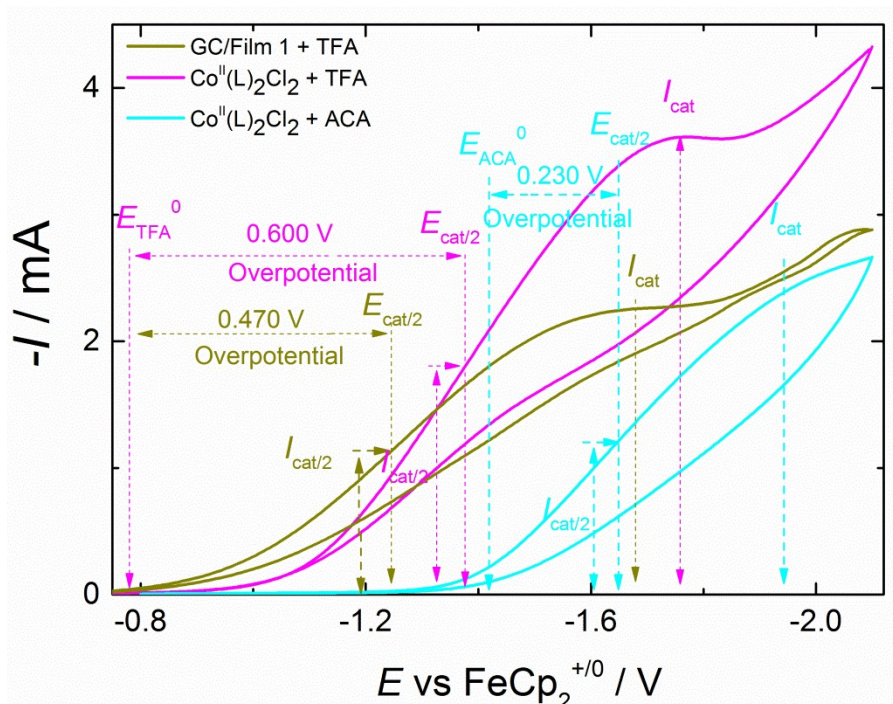


Figure S12. Cyclic voltammograms for GC modified with Film 1 (GC/Film 1) in the presence of 240 mM TFA; bare GC in the presence of 0.5 mM $\text{Co}^{\text{II}}(\text{L})_2\text{Cl}_2$ + 240 mM TFA, and 0.5 mM $\text{Co}^{\text{II}}(\text{L})_2\text{Cl}_2$ + 200 mM ACA. Potential scan rate: 20 mV s^{-1} . Potential scans begin at -0.75 V (negative direction). All experiments were conducted in N_2 -saturated $0.1 \text{ M TBAClO}_4/\text{ACN}$, with a polished surface for bare GC prior to the beginning of each CV.

Table S10. TOF and overpotential values for different complexes and materials.

Complex	TOF (s^{-1}) in ACN	Overpotential (mV)	Ref.
$\text{Co}^{\text{II}}(\text{L})_2\text{Cl}_2$	1900 in ACA; 4237.4 (corrected to 2754.3) in TFA	230 in ACA; 600 in TFA	Present study
Film 1	1.49×10^6 (corrected to 3.13×10^5) in TFA	470 in TFA	Present study
$[\text{Ni}(\text{P}^{\text{Ph}}_2\text{N}^{\text{C}_6\text{H}_4\text{OH}})_2]^{2+}$	750–170 000 in water(75%)–ACN solutions	310–470	[8]
$[\text{Ni}(\text{8P}^{\text{Ph}}_2\text{N}^{\text{C}_6\text{H}_4\text{Br}})_2]^{2+}$	800	700	[9]
$[\text{Ni}(\text{bdt})(\text{dppf})]$ (bdt = 1,2-benzenedithiolate, dppf = 1,1'-bis(diphenylphosphino)ferrocene)	1220–1290	265 at low acid concentration to 500 at high acid concentration	[10]
$[\text{Ni}(\text{P}^{\text{Ph}}_2\text{N}^{\text{Ph}})_2](\text{BF}_4)_2$	33 000 in dry ACN; 106 000 in the presence of 1.2 M of water	~625	[11]
$[\text{Ni}(\text{P}^{\text{Ph}}_2\text{N}^{\text{C}_6\text{H}_4\text{X}})_2](\text{BF}_4)_2$	<1.0 to 1850	230–380	[12]
$[\text{Ni}(\text{7P}^{\text{Ph}}_2\text{N}^{\text{H}})_2\text{H}]^{3+}$	160–780	320–470	[13]
$[\text{Ni}(\text{7P}^{\text{Ph}}_2\text{N}^{\text{C}_6\text{H}_4\text{X}})_2](\text{BF}_4)_2$	2400–27 000;	550–640	[14]

	4100–96 000 (in water up to 1.0 M)		
[Ni(L4)] ₂ ⁺ (L4 = 2,12-dimethyl-7-phenyl-3,11,17-triaza-7-phosphabicyclo[11,3,1]heptadecan-1(17),13,15-triene)	220	1070	[15]
[Co ^{III} (prdioXH)(^{4t} Bu ₃ py)(Cl)]PF ₆ , (^{4t} Bu ₃ py = <i>tert</i> -butyl-pyridino ligand and prdioXH = (2 <i>E</i> ,2' <i>E</i> ,3 <i>E</i> ,3' <i>E</i>)-3,3'-(propane-1,3-diylbis(azanylylidene))bis(butan-2-one)dioxime)	-	350	[16]
[Co ^{III} Br ₂ {(DO)(DOH)pn}], (DO)(DOH)pn = N ² ,N ^{2'} -propanediylbis(2,3-butanedione-2-imine-3-oxime)	-	250	[17]
Co(dmgbF ₂) ₂ (CH ₃ CN) ₂ , dmgbF ₂ = difluoroboryl-dimethylglyoxime	-	40	[18]
[Cp ^{C5F4N} Co ^{II} (P ^t Bu ₂ N ^{Ph} ₂)](BF ₄); (P ^t Bu ₂ N ^{Ph} ₂ = 1,5-diphenyl-3,7-ditert-butyl-1,5-diaza-3,7-diphosphacyclooctane and Cp ^{C5F4N} = C ₅ H ₄ (C ₅ F ₄ N))	360 (in water up to 0.56 M)	860	[19]
[Co ^{II} (P ^t Bu ₂ N ^{Ph} ₂)(CH ₃ CN) ₃] ²⁺ and Co ^{II} (dmgbF ₂) ₂ (CH ₃ CN) ₂	-	180–300	[20]
[Co(P ^{Ph} ₂ N ^{Ph} ₂)(CH ₃ CN) ₃](BF ₄) ₂	90	285	[21]
[Co(P ^{nC} -P ^{Ph} ₂ N ^{Ph} ₂)(CH ₃ CN)](BF ₄) ₂	980; 18 000 (with water addition)	930, 1210	[22]
[Co(S ₂ C ₂ Ar ₂) ₂] ₂	-	350	[23]
[Co ₃ (C ₅ H ₉ O ₂) ₆][BF ₄] ₂	80	300	[24]
Cobalt (II) - trisglyoximate clathrochelate	-	700	[25]
Film 2	-	606 vs RHE at 10 mA cm ⁻² in 0.5 M H ₂ SO ₄	Present study
P1-Co (CoS ₂ N ₂)	-	621 vs RHE at 10 mA cm ⁻² in 0.5 M H ₂ SO ₄	[26]
2D MOFs:THTA-Co	-	283 vs RHE at 10 mA cm ⁻² in 0.5 M H ₂ SO ₄	[27]
THTNi 2DSP	-	333 vs RHE at 10 mA cm ⁻² in 0.5 M H ₂ SO ₄	[28]
CNT/Co	-	590 vs RHE at 1 mA cm ⁻² in acetate buffer (0.1 M, pH 4.5)	[29]
Ni-functionalized GDL/MWCNT	-	300 vs NHE at 4 mA cm ⁻² in 0.5 M H ₂ SO ₄	[30]
Cobalt dithiolene polymer	-	580 vs RHE at 10 mA cm ⁻² in pH 1.3	[31]

		H ₂ SO ₄ solution	
Cobalt dithiolene polymer	-	340 and 530 vs SHE at 10 mA cm ⁻² in pH 1.3 H ₂ SO ₄ solution	[32]
PANI/CoP HNWs-CFs	-	~50 vs RHE at 10 mA cm ⁻² in 0.5 M H ₂ SO ₄	[33]
TiO ₂ NDs/Co NSNTs-CFs	114 at -0.3 V vs RHE in 1 M KOH	106 vs RHE at 10 mA cm ⁻² in 1 M KOH	[34]
Cu NDs/Ni ₃ S ₂ NTs-CFs	100 at -0.22 V vs RHE in 1 M KOH	128 vs RHE at 10 mA cm ⁻² in 1 M KOH	[35]

SHE = standard hydrogen electrode, NHE = normal hydrogen electrode

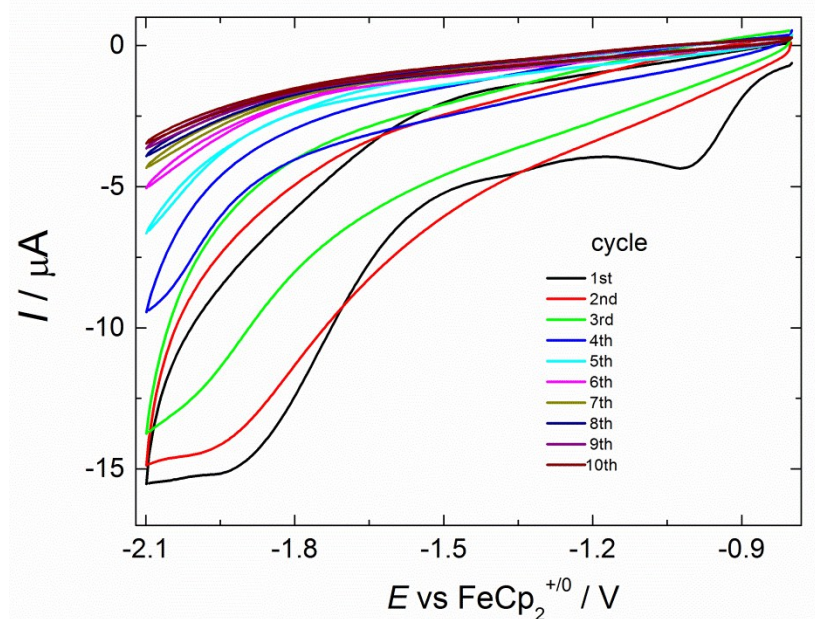


Figure S13. Continuous cyclic voltammograms for bare GC in the presence of 0.5 mM Co^{II}(L)₂Cl₂ in N₂-saturated 0.1 M TBAClO₄/ACN. Potential scan rate: 20 mV s⁻¹. Potential scans begin at -0.80 V (negative direction).

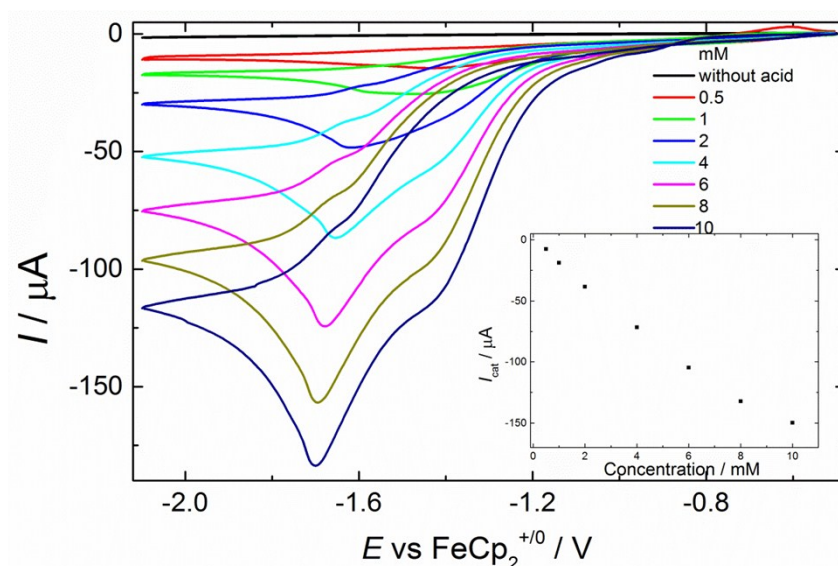


Figure S14. Cyclic voltammograms for GC modified with Film 1 (GC/Film 1) in the presence (or absence) of different concentrations of TFA. Inset: Cathodic catalytic peak currents for GC/Film 1 electrode in relation to TFA concentration. All experiments were carried out in N_2 -saturated 0.1 M $TBAClO_4/ACN$. Potential scan rate: 20 mV s^{-1} . Potential scans begin at -0.50 V in negative direction.

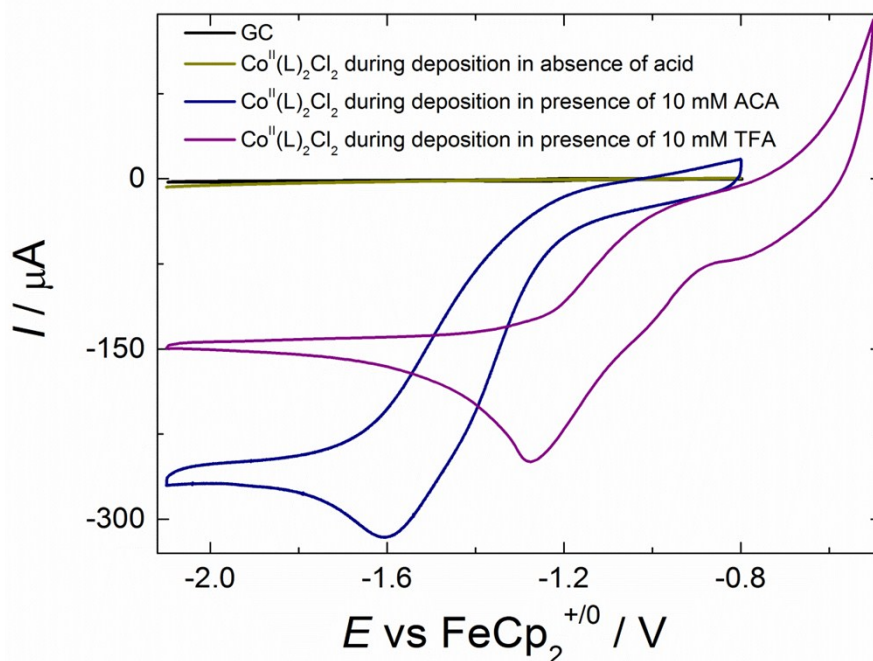


Figure S15. Cyclic voltammograms for bare GC, and 20 voltammetry cycles for the production of films after setting the potential at -2.1 V vs $FeCp_2^{0/+}$ for 1800 s followed by 20 cycles at 20 mV s^{-1} from -0.8 to -2.1 V vs $FeCp_2^{0/+}$ in a 0.1 M $TBAClO_4/ACN$ solution containing 0.5 mM $Co^{II}(L)_2Cl_2$ in the absence of acid (Film 1), in the presence of 10 mM ACA (Film 2), and in the presence of 10 mM TFA (Film 3, with VC from -0.5 to -2.1 V). All experiments were performed in N_2 -saturated 0.1 M $TBAClO_4/ACN$. Potential scan rate: 20 mV s^{-1} . Potential scans begin at -0.80 or -0.50 V in negative direction.

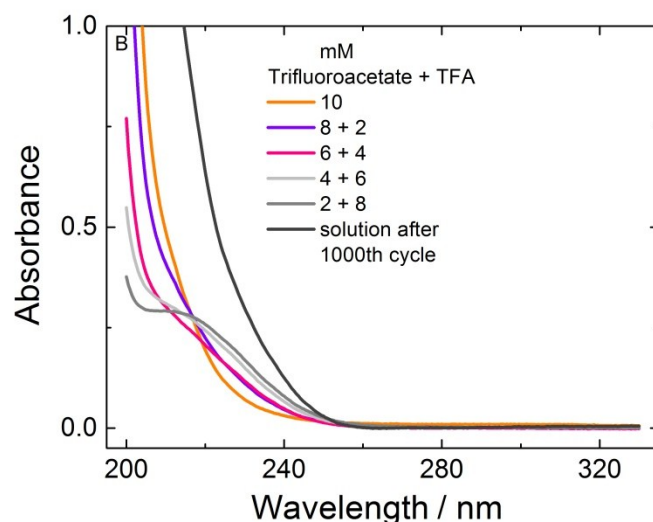


Figure S16. Absorbance versus wavelength for different concentrations of trifluoroacetate + TFA in 0.1 M TBAClO₄/ACN and 0.1 M TBAClO₄/ACN solution containing initially 10 mM of TFA, after 1000th cycle in the experiment shown in Figure 10. (Blank: 0.1 M TBAClO₄/ACN)

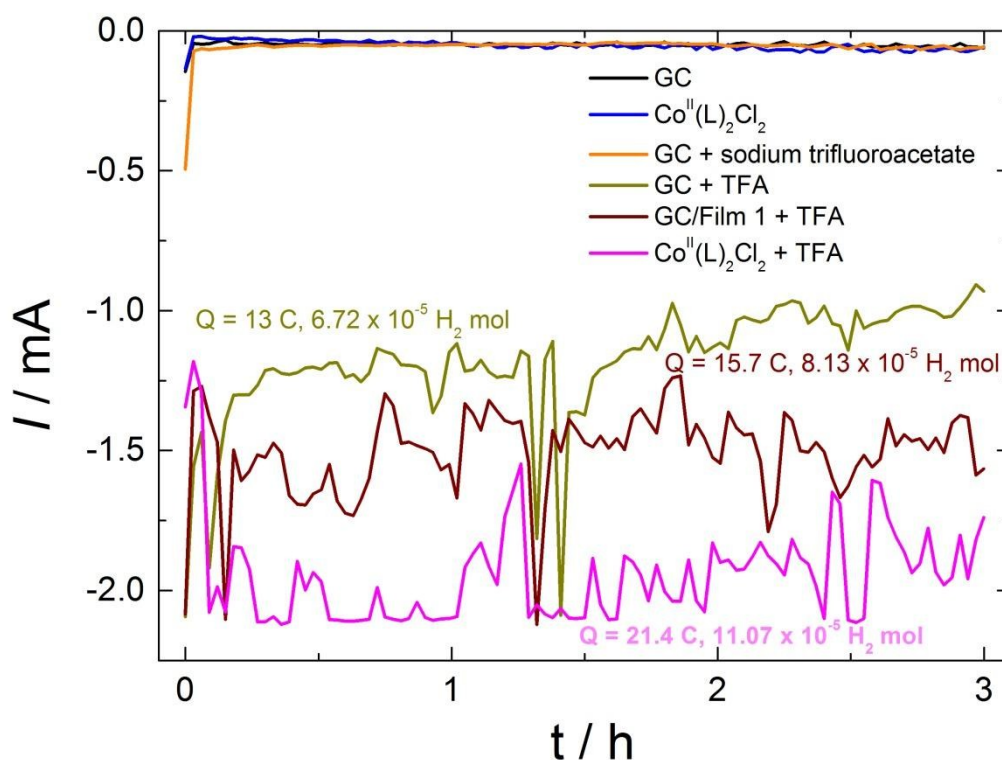


Figure S17. Chronoamperometric results for bare GC and bare GC in the presence of 0.5 mM Co^{II}(L)₂Cl₂, 240 mM sodium trifluoroacetate, 240 mM TFA, 0.5 mM Co(II)(L)₂Cl₂ + 240 mM TFA, and GC modified with Film 1 in presence of 240 mM TFA in 0.1 M TBAClO₄/ACN (before starting the experiments the solutions were N₂-saturated). Potential stepped from -0.5 to -1.6 V vs FcCp₂^{0/+} and kept at -1.6 V vs FcCp₂^{0/+} during 3 hours.

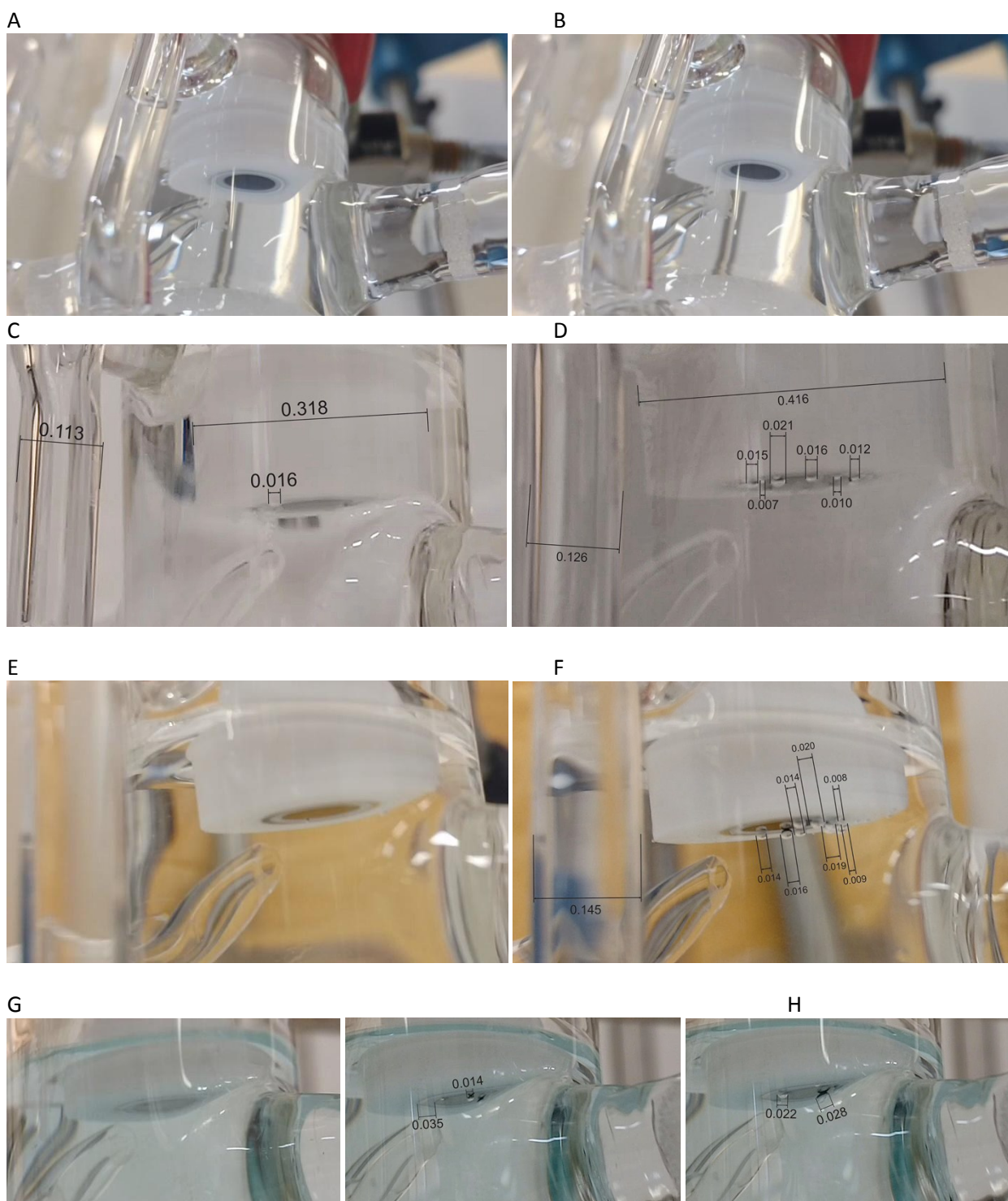


Figure S18. Photos of the H_2 bubbles caught from representative videos produced during the chronoamperometric measurements (Figure S17) where A, C, E, and G are referred to 0 min and B, D, F, and H are referred to 1 min. Bare GC in presence of 240 mM of sodium trifluoroacetate (photos A and B), bare GC in presence of 240 mM TFA (photos C and D), GC modified with Film 1 in presence of 240 mM TFA (photos E and F) and bare GC in presence of 0.5 mM $\text{Co}^{\text{II}}(\text{L})_2\text{Cl}_2 + 240$ mM TFA (photos G and H). The slight bluish color at photos from G to H is due to the presence of 0.5 mM $\text{Co}^{\text{II}}(\text{L})_2\text{Cl}_2$ in solution. The numbers on the photos were used to calculate the volume of sphere or half-sphere. Based in the diameter of the entire electrode (including the PTFE jacket) the number on the photos is related to 1.5 cm (diameter of the entire electrode, including the PTFE jacket). Based in the diameter of the glass tube (glass tube used to initial N_2 solution saturation) the number on the photos is related to 0.6 cm (real diameter of the glass tube). Authors' photographs.

Chronoamperometric measurements and calculation of the H₂ bubbles volume

The chronoamperometric measurements were conducted at a cell shown in Figure S19. The solution was N₂-saturated before the measurements, afterwards the cell was sealed.

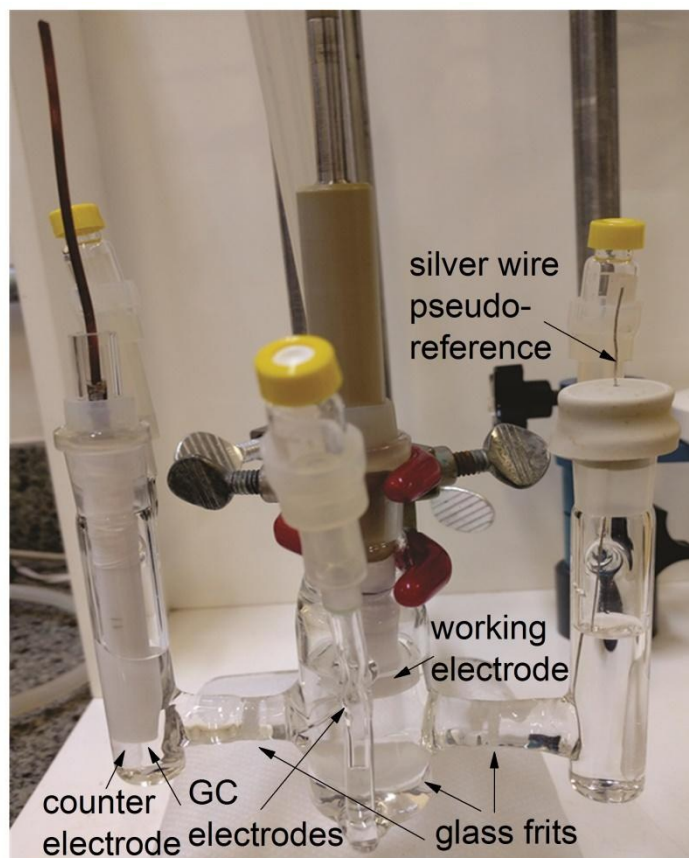


Figure S19. Photo of the three-compartment bulk electrolysis cell used for the electrolytic production of H₂. Authors' photograph.

The calculation of the hydrogen produced (bubbles of H₂) was based on the sphere volume ($\frac{4}{3}\pi r^3$) and/or half-sphere volume ($\frac{4}{6}\pi r^3$) considering an average value of several 1 minute of video images during the chronoamperometric measurement (see examples of photos representing 1 minute in the Figure S18) and multiplying this average value by 180 min that was the total time of chronoamperometric measurements. Aiming the calculation of the H₂ mol number produced, the total H₂ volume calculated in 180 min of experiment was used in the state equation of an ideal gas ($PV = nRT$, P = pressure, V = volume, n = number of moles, R = ideal gas constant, T = temperature in Kelvin [36]), assuming that the H₂ presents an ideal gas behavior and the experimental pressure and temperature were 1 atm and 25 °C respectively. The obtained volume of H₂ using the ideal gas equation was 0.070 cm³ resulting in $n_{\text{mol}} = 2.87 \times 10^{-6}$ mol for

bare GC in presence of TFA 240 mM. For GC modified with Film 1 in presence of TFA 240 mM, the obtained volume of H₂ using the ideal gas equation was 0.111 cm³ which results in $n_{\text{mol}} = 4.52 \times 10^{-6}$ H₂ mol and the volume of H₂ obtained using the ideal gas equation for bare GC in presence of 0.5 mM Co^{II}(L)₂Cl₂ + TFA 240 mM was 0.101 cm³ resulting in $n_{\text{mol}} = 4.14 \times 10^{-6}$ H₂ mol.

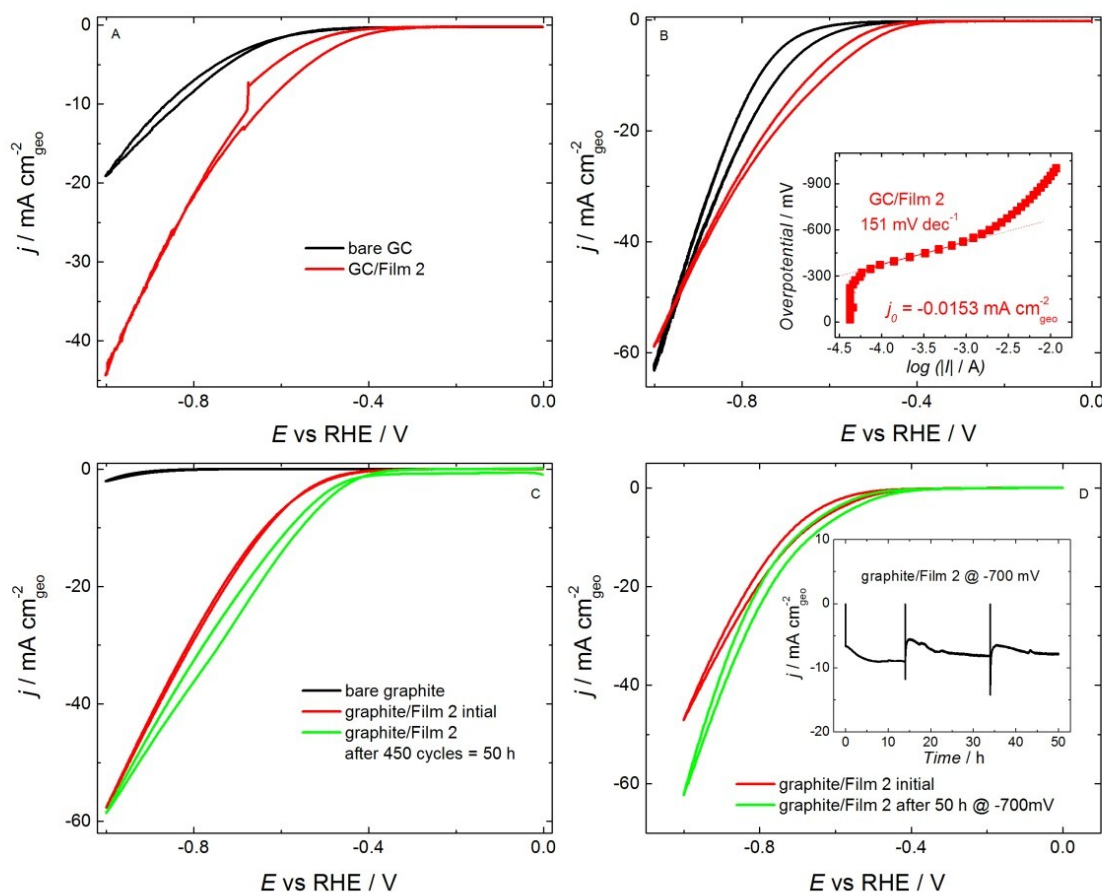


Figure S20. Cyclic voltammies (A) and hydrodynamic cyclic voltammies (B) recorded with bare GC and GC electrode modified with Film 2 in N₂-saturated 0.5 M H₂SO₄. Inset of Figure S20B: Tafel plot for GC electrode modified with Film 2 from curve in red of Figure S20B. Cyclic voltammies (C) recorded with bare graphite (2 cm² in geometric area), graphite electrode modified with Film 2, and graphite electrode modified with Film 2 after 450 cycles (50 h of cycling) in N₂-saturated 0.5 M H₂SO₄. Cyclic voltammies (D) recorded with graphite electrode modified with Film 2 and graphite electrode modified with Film 2 after 50 h at -700 mV vs RHE in N₂-saturated 0.5 M H₂SO₄. Inset of Figure S20D: Chronoamperometric result for a graphite electrode modified with Film 2 during 50 h at -700 mV vs RHE in N₂-saturated 0.5 M H₂SO₄. Scans started at 0.0 V. v: 5 mV s⁻¹, $\omega = 1600$ rpm.

CCDC 1581490 contains the supplementary crystallographic data for the Co^{II} complex. These data can be obtained free of charge via <http://www.ccdc.cam.ac.uk/conts/retrieving.html>, or from the Cambridge Crystallographic Data Center, 12 Union Road, Cambridge CB2 1EZ, UK; fax: (+44) 1223-336-033; or e-mail: deposit@ccdc.cam.ac.uk.

References

- [1] L. Pizzuti, L. A. Piovesan, A. F. C. Flores, F. H. Quina and C. M. P. Pereira, *Ultrason. Sonochem.*, 2009, **16**, 728-731.
- [2] A. Ferle, L. Pizzuti, S. D. Inglez, A. R. L. Caires, E. S. Lang, D. F. Back, A. F. C. Flores, A. M. Júnior, V. M. Deflon and G. A. Casagrande, *Polyhedron*, 2013, **63**, 9-14.
- [3] L. R. V. Favarin, P. P. Rosa, L. Pizzuti, A. M. Junior, A. R. L. Caires, L. Bezerra, L. M. C. Pinto, G. Maia, C. C. Gato, D. F. Back, A. Anjos and G. A. Casagrande, *Polyhedron*, 2017, **121**, 185-190.
- [4] B. D. McCarthy, D. J. Martin, E. S. Rountree, A. C. Ullman, J. L. Dempsey, *Inorg. Chem.*, 2014, **53**, 8350-8361.
- [5] V. Fourmond, P.-A. Jacques, M. Fontecave, V. Artero, *Inorg. Chem.*, 2010, **49**, 10338-10347.
- [6] J. A. S. Roberts, R. M. Bullock, *Inorg. Chem.*, 2013, **52**, 3823-3835.
- [7] A. M. Appel, M. L. Helm, *ACS Catal.*, 2014, **4**, 630-633.
- [8] R. M. Bullock, A. M. Appel and M. L. Helm, *Chem. Commun.*, 2014, **50**, 3125-3143.
- [9] S. Wiese, U. J. Kilgore, M.-H. Ho, S. Raugei, D. L. DuBois, R. M. Bullock and M. L. Helm, *ACS Catal.*, 2013, **3**, 2527-2535.
- [10] L. Gan, T. L. Groy, P. Tarakeshwar, S. K. S. Mazinani, J. Shearer, V. Mujica and A. K. Jones, *J. Am. Chem. Soc.*, 2015, **137**, 1109-1115.
- [11] M. L. Helm, M. P. Stewart, R. M. Bullock, M. R. DuBois and D. L. DuBois, *Science*, 2011, **333**, 863-866.
- [12] U. J. Kilgore, J. A. S. Roberts, D. H. Pool, A. M. Appel, M. P. Stewart, M. R. DuBois, W. G. Dougherty, W. S. Kassel, R. M. Bullock and D. L. DuBois, *J. Am. Chem. Soc.*, 2011, **133**, 5861-5872.
- [13] H. J. S. Brown, S. Wiese, J. A. S. Roberts, R. M. Bullock and M. L. Helm, *ACS Catal.*, 2015, **5**, 2116-2123.
- [14] M. P. Stewart, M.-H. Ho, S. Wiese, M. L. Lindstrom, C. E. Thogerson, S. Raugei, R. M. Bullock and M. L. Helm, *J. Am. Chem. Soc.*, 2013, **135**, 6033-6046.
- [15] L. Chen, G. Chen, C.-F. Leung, S.-M. Yiu, C.-C. Ko, E. Anxolabéhère-Mallart, M. Robert and T.-C. Lau, *ACS Catal.*, 2015, **5**, 356-364.
- [16] D. Basu, S. Mazumder, J. Niklas, H. Baydoun, D. Wanniarachchi, X. Shi, R. J. Staples, O. Poluektov, H. B. Schlegel and C. N. Verani, *Chem. Sci.*, 2016, **7**, 3264-3278.
- [17] N. M. Muresan, J. Willkomm, D. Mersch, Y. Vaynzof and E. Reisner, *Angew. Chem. Int. Ed.*, 2012, **51**, 12749-12753.
- [18] X. Hu, B. S. Brunschwig and J. C. Peters, *J. Am. Chem. Soc.*, 2007, **129**, 8988-8998.
- [19] M. Fang, E. S. Wiedner, W. G. Dougherty, W. S. Kassel, T. Liu, D. L. DuBois and R. M. Bullock, *Organometallics*, 2014, **33**, 5820-5833.

- [20] E. S. Wiedner and R. M. Bullock, *J. Am. Chem. Soc.*, 2016, **138**, 8309–8318.
- [21] G. M. Jacobsen, J. Y. Yang, B. Twamley, A. D. Wilson, R. M. Bullock, M. R. DuBois and D. L. DuBois, *Energy Environ. Sci.*, 2008, **1**, 167–174.
- [22] E. S. Wiedner, A. M. Appel, D. L. DuBois and R. M. Bullock, *Inorg. Chem.*, 2013, **52**, 14391–14403.
- [23] C. S. Letko, J. A. Panetier, M. Head-Gordon and T. D. Tilley, *J. Am. Chem. Soc.*, 2014, **136**, 9364–9376.
- [24] H. S. Ahn, T. C. Davenport and T. D. Tilley, *Chem. Commun.*, 2014, **50**, 3834–3837.
- [25] S. El Ghachtouli, M. Fournier, S. Cherdo, R. Guillot, M.-F. Charlot, E. Anxolabéhère-Mallart, M. Robert and A. Aukauloo, *J. Phys. Chem. C*, 2013, **117**, 17073–17077.
- [26] L. Wang, D. C. Tranca, J. Zhang, Y. Qi, S. Sfaelou, T. Zhang, R. Dong, X. Zhuang, Z. Zheng and G. Seifert, *Small*, 2017, **13**, 1700783.
- [27] R. Dong, Z. Zheng, D. C. Tranca, J. Zhang, N. Chandrasekhar, S. Liu, X. Zhuang, G. Seifert and X. Feng, *Chem. Eur. J.*, 2017, **23**, 2255–2260.
- [28] R. Dong, M. Pfeffermann, H. Liang, Z. Zheng, X. Zhu, J. Zhang and X. Feng, *Angew. Chem. Int. Ed.*, 2015, **54**, 2058–12063.
- [29] E. S. Andreiadis, P.-A. Jacques, P. D. Tran, A. Leyris, M. Chavarot-Kerlidou, B. Jusselme, M. Matheron, J. Pécaut, S. Palacin, M. Fontecave and V. Artero, *Nat. Chem.*, 2013, **5**, 48–53.
- [30] A. L. Goff, V. Artero, B. Jusselme, P. D. Tran, N. Guillet, R. Métayé, A. Fihri, S. Palacin, M. Fontecave, *Science*, 2009, **326**, 1384–1387.
- [31] C. A. Downes and S. C. Marinescu, *J. Am. Chem. Soc.*, 2015, **137**, 13740–13743.
- [32] A. J. Clough, J. W. Yoo, M. H. Mecklenburg and S. C. Marinescu, *J. Am. Chem. Soc.*, 2015, **137**, 118–121.
- [33] J.-X. Feng, S.-Y. Tong, Y.-X. Tong and G.-R. Li, *J. Am. Chem. Soc.*, 2018, **140**, 5118–5126.
- [34] J.-X. Feng, H. Xu, Y.-T. Dong, X.-F. Lu, Y.-X. Tong and G.-R. Li, *Angew. Chem. Int. Ed.*, 2017, **56**, 2960–2964.
- [35] J.-X. Feng, J.-Q. Wu, Y.-X. Tong and G.-R. Li, *J. Am. Chem. Soc.*, 2018, **140**, 610–617.
- [36] I. N. Levine, *Physical Chemistry*, McGraw-Hill Book Company, New York, third edition, 1998.